Publication P2

Jere Kolehmainen and Jouni Ikäheimo. 2008. Motors with buried magnets for medium-speed applications. IEEE Transactions on Energy Conversion, volume 23, number 1, pages 86-91.

Motors With Buried Magnets for Medium-Speed Applications

Jere Kolehmainen and Jouni Ikäheimo

***Abstract*—A novel type of mechanically robust buried magnet rotor structure is proposed for medium speed permanent magnet machines. A machine utilizing the construction is built, tested, and compared to another machine with traditional V-shaped poles. The machine is also simulated using finite element method and the results are compared to tested values. The obtained results demonstrate the feasibility of the construction.**

***Index Terms*—Electromagnetic analysis, permanent magnet machines, synchronous machines, variable speed drives.**

I. Introduction

PERMANENT magnet synchronous motors (PMSM) with buried magnets have been considered in a wide range of variable speed drives [1]–[4]. A buried magnet design has many advantages compared to designs with surface mounted and inset magnets. With a buried magnet design, flux concentration can be achieved, which induces higher air gap flux density. That, in turn, gives a possibility to increase torque of a machine. The buried magnet construction also gives a possibility to create a nonuniform air gap resulting smoother torque [5]–[7] and more sinusoidal currents [8], [9]. Different types of buried magnet rotors can be seen in Fig. 1.

The typical way of manufacture a buried PM rotor is to assemble a stack of punched rotor disks with rectangular holes and insert magnets into these holes. The rotor poles between the magnets are fixed to rest of the rotor structure with thin iron bridges (see details x in Fig. 1). The disadvantage of the supporting bridges is the leakage flux [10], the magnitude of which depends on the thickness of the bridges. In low-speed applications, this is not a problem since the centrifugal forces acting on the poles are relatively small and the bridges can be kept thin. However, as the tangential speed of the rotor surface in medium-speed applications (4000–8000 min^{-1}) exceeds 50 m/s (corresponding to 4000 min^{-1} in motor size IEC250), the stress in the bridges will exceed the yield strength of the electrical steel (typically 300 MPa for grade M400–50 A). The problem can be countered by increasing the thickness of the bridges, however, this increases the leakage flux, which, in turn, increases the amount of magnet material needed to get the required torque.

In this paper, we study a solution on how to get mechanically more robust rotor structures using thin iron bridges. In the solution, the tensile stress is geometrically converted into compressive one, and the magnets are used to support the pole structure. The new solution is compared to a traditionally used solution with V-shaped poles. The comparison is done using time stepping and static calculations using finite element method (FEM) [11]. Motors with both the rotor designs are built and tested. The motor with the new dovetail pole design is analyzed further and results are compared to simulations.

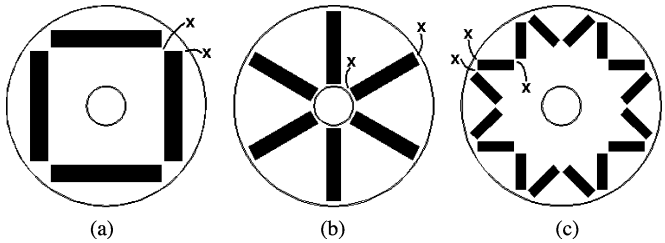

Fig. 1. Rotor constructions of buried permanent magnet motors with (a) tangential magnets, (b) radial magnets, and (c) V-shaped magnet poles.

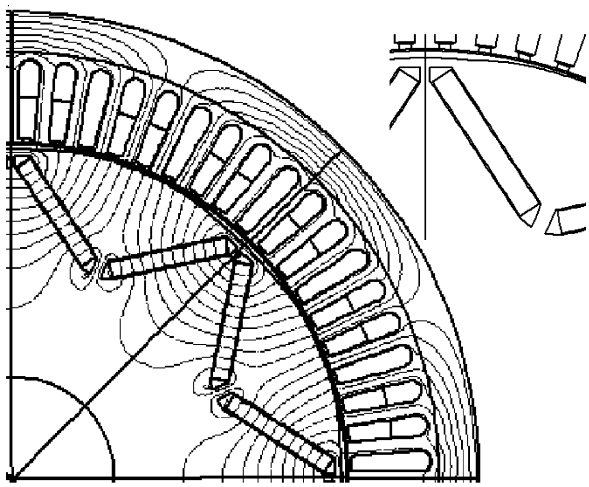

Fig. 2. Design with V-shaped poles with flux lines created by the remanence flux of the magnets. Details without flux lines are shown top right.

II. Rotor Design

An eight-pole motor with V-shaped poles in the rotor [see Fig. 1(c)] is used as an example for comparison to a motor with the new dovetail design. The only difference of the two motors is in their rotor structure. The rotor geometries can be seen in Figs. 2 and 3. An eight-pole motor has eight symmetry sections in V-pole design, but in the new dovetail design, the rotor has magnets in every second pole. The pole consists of three magnets (the V-pole design has two) and the wedge-like pole shoe, which narrows toward the air gap. As the centrifugal force pushes the

Manuscript received October 9, 2006; revised January 26, 2007. This work was supported in part by the ABB Oy, Motors, Finland. Paper no. TEC-00475-2006.

The authors are with the ABB Oy, Motors, Vaasa 65101, Finland (e-mail: jere.kolehmainen@fi.abb.com; jouni.ikaheimo@fi.abb.com).

Digital Object Identifier 10.1109/TEC.2007.914331

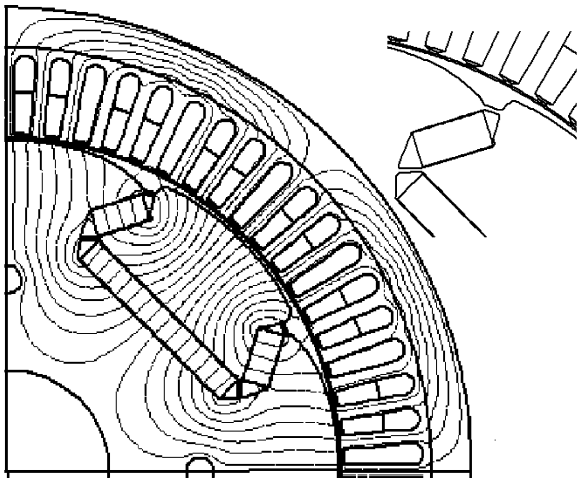

Fig. 3. New design with dovetail shaped poles with flux lines created by the remanence flux of the magnets. Details without flux lines are shown top right.

TABLE I
NOMINAL VALUES AND MAIN DIMENSIONS OF STUDIED MACHINES

Quantity	Value
Shaft height (mm)	250
Power (kW)	185
Torque (Nm)	440
Voltage (V)	460
Current (A)	242
Speed (rpm)	4000
Stator outer radius (mm)	205
Stator inner radius (mm)	147.5
Stack length (mm)	165
Air gap (mm)	1.2
Number of poles	8
Number of slots per pole per phase	6
Connection	Delta
Number of effective conductors in slot	3.5
Number of parallel branches	4

pole shoe radially outwards, the smaller magnets lock the pole firmly in place and prevent it from moving. Although the modern PM materials are rather brittle, the magnets tolerate *compressive* stress surprisingly well (up to 800 MPa). Simultaneously, the large contact area between the pole wedge and the magnets renders the compressive stress to an acceptable level.

The studied motors are designed to work with speed of 4000 min^{-1} and torque 440 N·m. The common machine data is shown in Table I.

There is slightly more magnetic material in the machine with dovetail design than in the machine with V-pole design. The magnet material, Neorem 495 a, is sintered Nd–Fe–B [12]. Magnet material data and dimensions of the magnets are shown in Table II.

III. SIMULATION RESULTS

Next, the electrical properties of the motors with original V-pole design in Fig. 2 and the new dovetail design in Fig. 3 are studied. The simulations are done in voltage source operation mode and in open circuit mode using Flux2D software by Cedrat Research [11]. Delta connection is used. The circuit of voltage source calculations is shown in Fig. 4. In the circuit, there are three voltage sources *U1*, *U2*, and *U3*, six windings *W*, three end-winding resistances *R*, and three end-winding inductances *L*. In all time stepping calculations with voltage source, the form of the voltage is sinusoidal and amplitude is kept the same. Simulations are started with various rotor angles and stopped after 54 electric periods when transient oscillations have totally died away. Constant rotor speed is used.

First, the machines are simulated in the open circuit mode: in the circuit described in Fig. 4 the voltage sources are replaced with infinite resistances. The flux lines due to the remanence flux of the magnets are shown in Figs. 2 and 3. Fig. 5 depicts the magnitude of the flux as a function of time in a stator tooth.

TABLE II
MAGNET MATERIAL AND DIMENSIONS OF MAGNETS

Quantity	V-design	Dovetail design
Remanence flux density (T)	1.1	
Energy product (kJ/m^3)	230	
Relative permeability	1.05	
Thickness (mm)	7.3	11.7
Area per pole (mm^2)	759	790
Width of pole (mm) (Area per pole/Thickness)	104	135
Total volume (dm^3)	1.002	1.043
Total mass (kg)	7.62	7.92

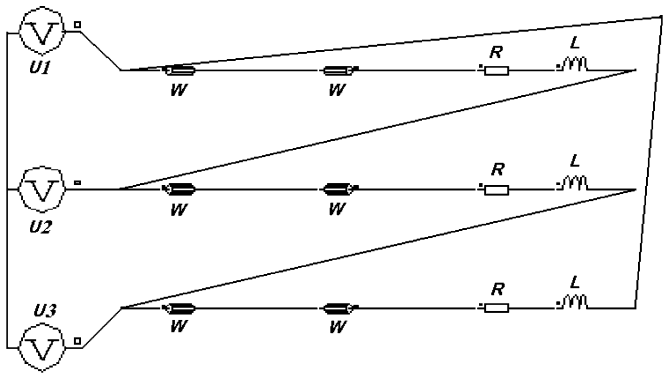

Fig. 4. Flux2D circuit used in the calculations.

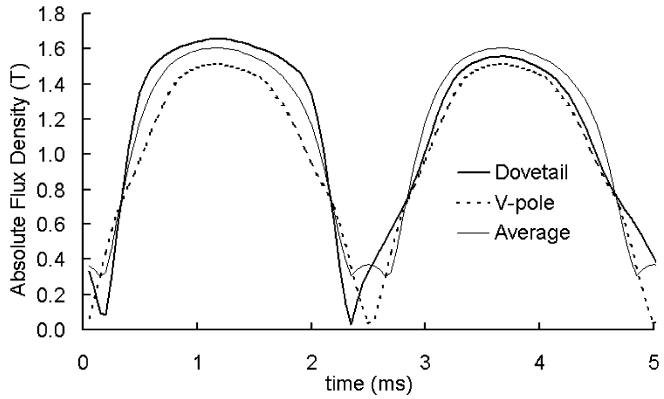

Fig. 5. Absolute flux densities in the stator teeth of V-pole and new dovetail designs produced by the remanence flux of the magnets when the rotor is rotating at 4000 min^{-1}. Average flux density of two poles of dovetail design is also shown.

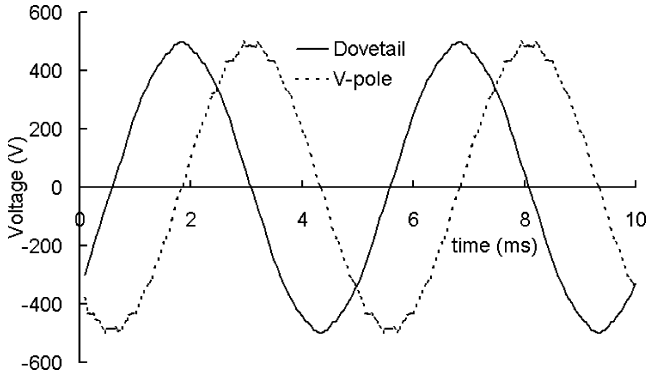

Fig. 6. Calculated voltage (open circuit and speed 4000 min^{-1}) of V-pole and new dovetail designs as a function of time.

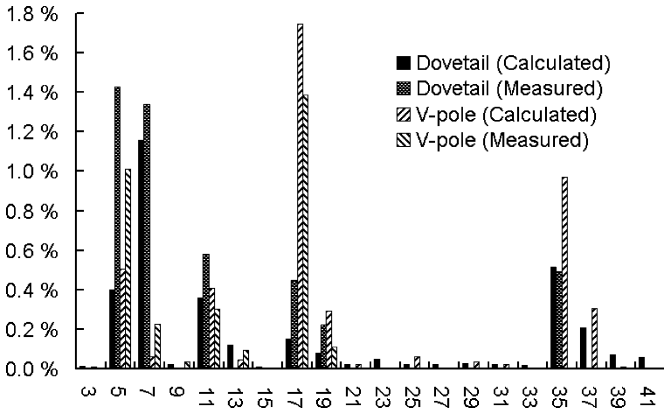

Fig. 7. Calculated and measured voltage harmonics (open circuit and speed 4000 min^{-1}) of V-pole and new dovetail designs.

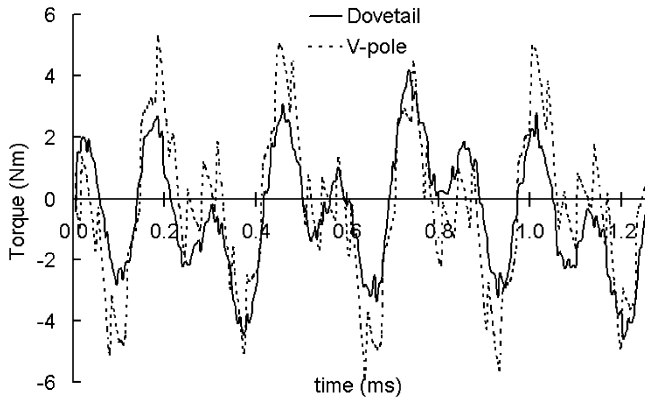

Fig. 8. Torque ripple (open circuit) of V-pole and new dovetail designs as a function of time (speed 4000 min^{-1}).

In the dovetail design, the asymmetric flux of the poles can be seen. Also, the average flux density of two poles of the dovetail design is shown in the figure. It is symmetric as can be expected.

The open circuit voltage as a function of time is shown in Fig. 6. Harmonics of these voltages are shown in Fig. 7. The biggest difference between harmonics of the two machines is in their 7th and 17th harmonics. The 7th harmonic is larger in the dovetail structure and the 17th harmonic is larger in the V-pole structure.

TABLE III
SIMULATED MACHINE DATA

Quantity	V-design	Dovetail design
Voltage (V)	460	460
Torque (Nm)	440	440
Current (A)	246.6	256.4
Efficiency (%) (Only copper and iron losses are taken into account)	0.979	0.975
Power factor	0.958	0.925
Maximum torque (Nm)	788	620
Current at maximum torque (A)	592	480

TABLE IV
PATHS OF FLUX IN ROTOR

Path of flux	V-design	Dovetail design
Magnets (mWb;%)	13.5; 100.0	16.3; 100.0
Bridges near air gap (mWb;%)	3.0; 13.6	3.2; 15.7
Bridges deep (mWb;%)	2.3; 16.8	2.5; 20.2
Air gap (mWb;%)	8.2; 69.6	10.6; 64.1

The torque ripple has similar behavior in both V-pole and dovetail designs, as can be seen in Fig. 8. The peaks have slightly higher amplitude in the V-pole design due to the different shape of the air gap. By tuning the shape of the poles, it is possible to make amplitude of the torque ripple even smaller.

The next computation is the simulation of the nominal load point. The evaluated values for the machine parameters are shown in Table III. In the efficiency calculations, only electromagnetic losses are taken into account. Iron losses are calculated from the equation

$$P_{\mathrm{TOT}} = k_h B_m^2 f + \frac{1}{T}\int_0^T \left[\sigma \frac{d^2}{12}\left(\frac{dB}{dt}(t)\right)^2 + k_e\left(\frac{dB}{dt}(t)\right)^{3/2}\right] k_f \, dt \quad (1)$$

where B_m is the maximum flux density at the node concerned, f is the frequency, σ is the conductivity, d is the lamination thickness, k_h is the coefficient of hysteresis loss, and k_e is the coefficient of excess loss.

It can be seen that maximum torque of the dovetail design is 21% smaller compared to the V design. This is because of the smaller total magnet thickness per pole, which results in a lower reluctance torque for the dovetail design compared to V design. In the dovetail design there is also a 5.5% higher leakage fluxes in iron bridges. Values of the leakage fluxes are given in Table IV.

Flux lines at nominal load are shown in Figs. 9 and 10. The concentration of the flux to the one side of the pole can be seen. Flux densities of the original and the new design at nominal load in a stator tooth as a function of time are shown in Fig. 11. At nominal load, different pole width and flux concentration in dovetail design results in a smaller torque oscillation as can be seen in Fig. 12. In the V design, there is a 4.5% torque oscillation coming from the stator slots. The dovetail design reduces this oscillation to 0.9% although this oscillation can be reduced also with skewing. However, our designs are not skewed. In the V-pole and the dovetail designs, the torque oscillations are almost the same (2.6% and 2.4%, correspondingly).

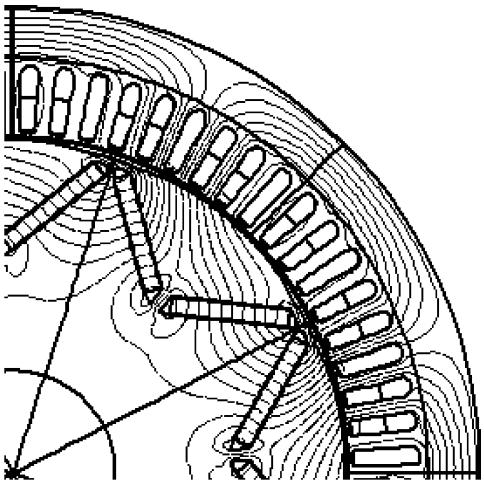

Fig. 9. Concentration of flux in the V-pole design at nominal operation point.

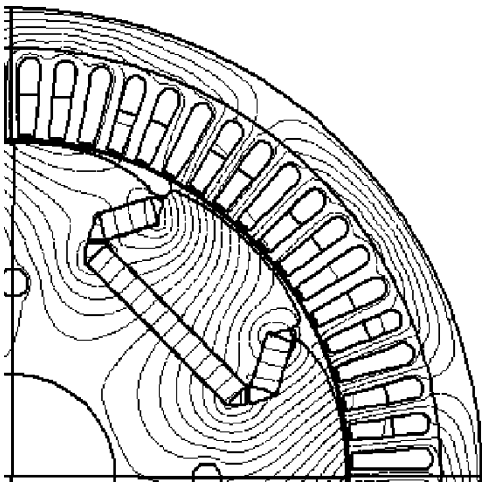

Fig. 10. Concentration of flux in the new dovetail design at nominal operation point.

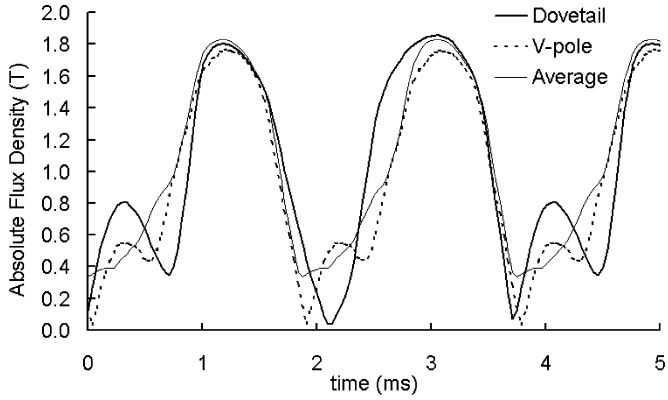

Fig. 11. Flux densities of V-pole and new dovetail designs at nominal load and speed 4000 min^{-1} in the stator teeth as a function of time.

In previous calculations, total torque in air gap is calculated with the virtual work method [13]. For an exact solution, torque per axial length is obtained from the Maxwell stress formula

$$T_e = \frac{1}{\mu_0} r^2 \int_0^{2\pi} B_r B_\varphi \, d\varphi \tag{2}$$

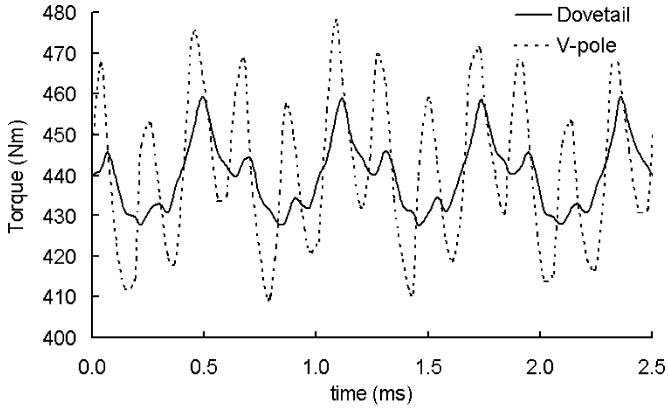

Fig. 12. Torque oscillations in V-pole and new dovetail designs at nominal load and speed 4000 min^{-1} as a function of time.

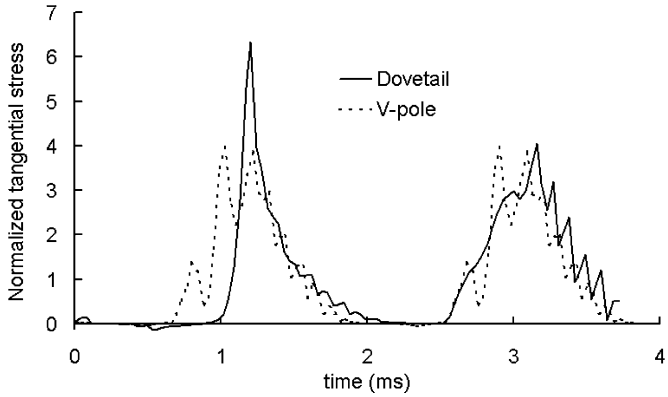

Fig. 13. Time distributions of normalized local Maxwell's stress in air gap of V-pole and new dovetail designs with nominal load and speed 4000 min^{-1} as a function of time.

where $B_r = B_r(r, \varphi)$ and $B_\varphi = B_\varphi(r, \varphi)$ are the r- and φ-components of the flux density. The local tangential Maxwell's stress

$$\sigma_{\tan} = \frac{1}{\mu_0} r^2 B_r B_\varphi . \tag{3}$$

To analyze tangential force distribution in air gap, the normalized local tangential Maxwell's stress is written as

$$\sigma_{\tan}^{\text{normalized}} = \frac{\sigma_{\tan}}{\int_0^T \sigma_{\tan} \, dt} = \frac{B_r B_\varphi}{\int_0^T B_r B_\varphi \, dt} \tag{4}$$

where T is time for one electric period. This equation gives possibility to analyze tangential stress distribution in the air gap without direct effect of the stator slots. Fig. 13 presents the normalized local tangential Maxwell's stress in one point of air gap by using (4) of V-pole and new dovetail designs between two stator slots for a function of time.

Despite the sharper stress distribution in every second pole with dovetail design, the torque oscillation is slightly smaller. The skewing, which is not taken into account in the simulations but is present in the actual machines, diminishes the difference to an insignificant level.

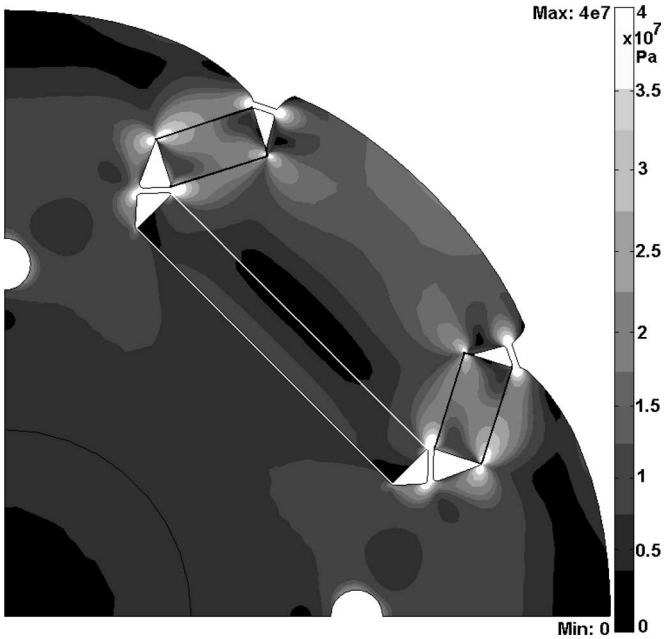

Fig. 14. Von Mises stress in the rotor with new dovetail design at speed 4000 min^{-1}.

IV. Force Computation

The rotor with a new dovetail design has a totally different stress distribution compared to the V-pole rotor. In the V-pole rotor, all of the shear and tension stresses are in the iron bridges whereas in the dovetail design, most of stresses are compression stress in the magnets and shear stress near corners of magnets. Von Mises stresses in the dovetail design with thin iron bridges are shown in Fig. 14. Computation is done using the centrifugal force associated with the speed of 4000 min^{-1}. In the figure, the stresses are greatest in light grey areas.

In the bridges of electrical steel sheet, the stress is about 115 MPa. The largest stress, 200 MPa, is locally in the corners of sheets. These values are below the yield strength (305 MPa) of the steel. In center of the smaller magnets, the stress is 18 MPa. It is well below the maximum compressive strength of the magnets. The calculated maximum stress in magnets is 110 MPa (located in corners). The magnets contribute to the force supporting the pole by 57% of the total; the rest of the force is in the bridges. Hence, without supporting magnets, the stress in the bridges would exceed the yield strength. Using magnets to stabilize the structure, it becomes robust enough for the speed of 4000 min^{-1}.

V. Test Results

Two machines with both rotor types are manufactured. The rotors without the magnets can be seen in Fig. 15. The general method to manufacture the rotor is to assemble a stack of disks, compress it using bolts and nonmagnetic end plates, and shrink fit the stack on the shaft. After that, the magnets are inserted into their holes using glue.

Fig. 15. Rotor stacks without magnets.

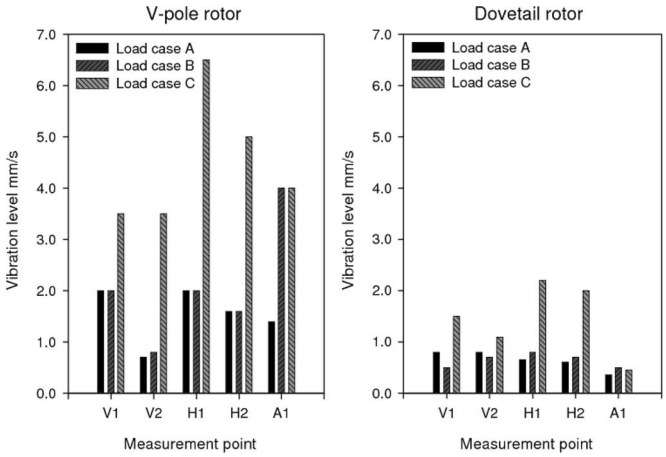

Fig. 16. Vibration levels of motors with the V-pole and the dovetail rotors. The abbreviations for measurement points V1, V2, H1, H2, and A1 stand for vertical 1, vertical 2, horizontal 1, horizontal 2, and axial 1, correspondingly. See the text for the description of the load cases A, B, and C.

For all tests, as for our industrial cases, the direct torque control strategy with software for permanent magnet ac machines is used with frequency converter ACS600 [14].

The mechanical durability test of the motors consists of three parts. First, the motor is tested at no load running at 4000 min^{-1} (load case A in Fig. 16). After this, the load is increased to the nominal level and the motors are run for 4 h (load case B). Finally, an over speed test is done by running the motors at 5500 min^{-1} for 3 min (load case C). Fig. 16 shows that the dovetail rotor maintains its balance much better the V-pole rotor, in which the vibration level clearly increases during the over speed test. Subsequential measurements revealed that the increase of the vibration level was irreversible, indicating plastic deformation in the rotor sheets.

The open circuit voltages with both designs were measured at the speed of 4000 min^{-1} and analyzed with Fourier transform. The measured and calculated harmonics are shown in Fig. 7. With both rotor designs, the measured 7th, 11th, and 17th

TABLE V
COMPARISON OF MEASURED AND CALCULATED PARAMETERS FOR THE DOVETAIL DESIGN

Quantity	Measured	Calculated
Voltage (V)	400	400
Torque (Nm)	276	277
Current (A)	192.6	171.3
Maximum torque (Nm)	400*	497
Current with maximum torque (A)		420
Open circuit voltage (V)	389.2	437.6

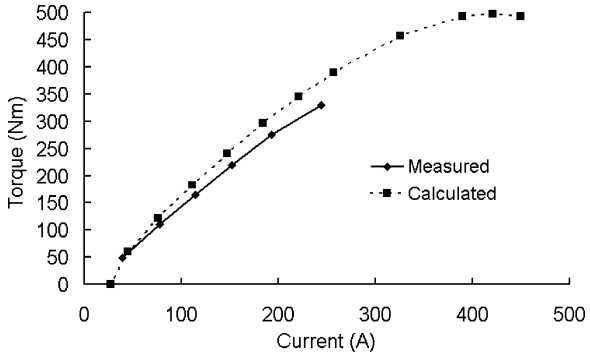

Fig. 17. Calculated and measured torque of the dovetail design as a function of current.

harmonics are same order of magnitude as the calculated values. The measured fifth harmonics are remarkably larger than the calculated ones in both the designs.

The load tests are done with a brake motor. The motor with dovetail design is tested with different loads at the speed of 4000 min^{-1}. First harmonic of motor terminal voltage was 400 V. With this voltage, the frequency converter allowed loading of the machine up to 330 N·m. The measured torque as a function of current is compared to calculated one in Fig. 17. Table V shows the measured and calculated values at the speed of 4000 min^{-1} and 400 V. Measured currents shown are root mean square values of first harmonic. Total harmonics distortion of measured currents is between 7.9% and 10.2% for cases with torque between 165 and 330 N·m while it is only 0.02% for the calculated case with torque 330 N·m. Practically, the measured current waveform is sinusoidal.

The actual motor has higher measured current than in the calculations. The calculated open circuit voltage is 12% larger than measured. The calculated maximum torque is also larger than measured torque, which is measured with pull into synchronism method [15]. Despite of this, the accuracy of the simulation is sufficient for the comparison of different rotor structures.

VI. CONCLUSION

The prototype motor with a dovetail-shaped magnet poles exhibits a significant increase in mechanical stability over the conventional V-pole design. By converting the tensile stress in the iron bridges into a compressive stress in the magnets by redesigning the pole geometry, a very robust construction can be achieved. The electrical properties and the consumption of magnetic material can be kept on the same level as in the V-pole design. Compared to the surface mounted magnet rotors, which are often encountered in high- and medium-speed applications, our design requires no pretension bandage to counter the centrifugal forces and is consequentially more straightforward to manufacture.

REFERENCES

[1] K. J. Tseng and S. B. Wee, "Analysis of flux distribution and core losses in interior permanent magnet motor," *IEEE Trans. Energy Convers.*, vol. 14, no. 4, pp. 969–975, Dec. 1999.
[2] B. K. Bose, "A high-performance inverter-fed drive system of an interior permanent magnet synchronous machine," *IEEE Trans. Ind. Appl.*, vol. 44, no. 6, pp. 987–997, Nov. 1988.
[3] E. C. Lovelace, T. M. Jahns, and J. H. Lang, "Impact of saturation and inverter cost on interior PM synchronous machine drive optimization," *IEEE Trans. Ind. Appl.*, vol. 36, no. 3, pp. 723–729, May/Jun. 2000.
[4] T. Ohnishi and N. Takahashi, "Optimal design of efficient IPM motor using finite element method," *IEEE Trans. Magn.*, vol. 36, no. 5, pp. 3537–3539, Sep. 2000.
[5] T. Li and G. Slemon, "Reduction of cogging torque in permanent magnet motors," *IEEE Trans. Magn.*, vol. 24, no. 6, pp. 2901–2903, Nov. 1998.
[6] T. Ishikawa and G. Slemon, "A method of reducing ripple torque in permanent magnet motors without skewing," *IEEE Trans. Magn.*, vol. 29, no. 2, pp. 2028–2031, Mar. 1993.
[7] F. Colamartimo, C. Marcand, and A. Razek, "Torque ripple minimization in permanent magnet synchronous servo drive," *IEEE Trans. Energy Convers.*, vol. 14, no. 3, pp. 616–621, Sep. 1999.
[8] J. Kolehmainen, "Finite element analysis of two PM-motors with buried magnets," presented at the ICEM. Krakow, Poland, 2004 (Springer, 2006, pp. 51–58. S. Wiak, M. Dems, and K. Komeza, Eds., *Recent Developments of Electrical Drives,* Nov. 2006).
[9] J. Salo, T. Heikkilä, J. Pyrhönen, and T. Haring, "New low-speed high-torque permanent magnet synchronous machine with buried magnets," presented at the ICEM. Espoo, Finland, 2000.
[10] W. Tsai and T. Chang, "Analysis of flux leakage in a brushless permanent-magnet motor with embedded magnets," *IEEE Trans. Magn.*, vol. 35, no. 1, pp. 543–547, Jan. 1999.
[11] Flux2D software. (2007). [Online]. Available: www.cedrat.com
[12] Neorem495s, Neorem Magnets. (2007). [Online]. Available: www.neorem.fi
[13] J. L. Coulomb, "A methodology for the determination of global electromechanical quantitxies from a finite element analysis and its applications to the evaluation of magnetic forces, torques and stiffness," *IEEE Trans. Magn.*, vol. 19, no. 6, pp. 2514–2519, Nov. 1983.
[14] ACS 607–0400-5. (2007). Frequency Converter [Online]. Available: www.abb. com
[15] P. K. Kovács, *Transient Phenomena in Electrical Machines*. Budapest, Hungary: Elsevier, 1984, vol. 9.

Jere Kolehmainen received the M.Sc. and Ph.D. degrees in theoretical physics from the University of Jyväskylä, Jyväskylä, Finland, in 1996 and 2000, respectively.

He is currently with ABB Oy, Motors, Vaasa, Finland. His current research interests include synchronous and induction ac machines and electromagnetic modeling.

Jouni Ikäheimo received the M.Sc. and Ph.D. degrees in theoretical physics from Helsinki University of Technology, Espoo, Finland, in 1992 and 1996, respectively.

He is currently an R&D manager with ABB Oy, Motors, Vaasa, Finland.